AIChE

Contraction of Free Liquid Ligaments

Ri Li, Nasser Ashgriz, and Sanjeev Chandra
Dept. of Mechanical and Industrial Engineering, University of Toronto, Toronto, ON, Canada M5S 3G8

John R. Andrews
Xerox Corporation, Wilson Center for Research and Technology, Webster, NY 14580

DOI 10.1002/aic.11619
Published online October 29, 2008 in Wiley InterScience (www.interscience.wiley.com).

This article presents an experimental and theoretical study on the contraction of free, stable, and inviscid liquid ligaments under the action of surface tension forces. The ligament is considered as two blobs of arbitrary initial sizes connected by a central column with a constant and uniform radius. Based on the conservation of mass, momentum, and energy, a theoretical model is developed to predict the ligament length as a function of time, thereby predicting the lifetime of the ligament. The theoretical results are compared with our experimental measurements of the transient length of liquid ligaments ejected from an inkjet printhead, showing good agreement. © 2008 American Institute of Chemical Engineers *AIChE J,* 54: 3084–3091, 2008
Keywords: contraction, liquid ligament, momentum conservation, energy conservation

Introduction

The contraction of liquid ligaments is an integral part of droplet formation in many engineering processes, such as in ink-jet printers[1] and pneumatic droplet generators.[2] Ligament contraction is also observed in a variety of hydrodynamic processes, including pinch-off of pendant drops,[3–6] relaxation of symmetrically elongated drops,[7–10] and droplet collision.[11–13]

Ligament contraction is a classical free-boundary problem, in which the ligament end tends to retract due to surface tension forces. Figure 1 schematically shows one end of a ligament with radius R retracting with velocity U. This problem has much similarity to the rim motion of disintegrated liquid sheets[14] and punctured liquid films.[15,16] The motion of liquid rim can also be represented by Figure 1, if we consider the schematic as a cross-section of a liquid sheet.

The available theoretical studies on ligament contraction are based on an approximate solution to the Navier-Stokes equations.[9,17–19] These studies report several contraction behaviors: (1) stable contraction; (2) breakup caused by end-pinching; (3) breakup caused by capillary instability. Schulkes[18] used a finite-element discretization procedure to investigate the contraction of liquid ligaments. The study showed a crucial dependence of dynamic characteristics of ligaments on the Ohnesorge number given by

$$Oh = \frac{\mu}{\sqrt{\rho\sigma R}}$$

where μ, ρ, σ are viscosity, density, and surface tension of the ligament, respectively. For $Oh > 1$, although the initial length of ligaments was larger than $2\pi R$ (the cutoff wavelength of capillary instability of infinite jets), the liquid ligament remained stable throughout the contraction process. Additionally, unless $Oh < 0.1$, end-pinching was not observed. Stone et al.[8] related the contraction dynamics to the ratio of ligament viscosity to the viscosity of ambient fluid. It was found that when this ratio was larger than 10, the contraction proceeded with constant diameter without breakup caused either by end-pinching or capillary instability.

This work is focused on the stable contraction of liquid ligaments with two free ends. From the standpoint of engineering applications, the length and lifetime of ligaments are of importance. For example, in a droplet dispensing system, the ligament length changing with time determines the location of the substrate where spherical droplets can be

Correspondence concerning this article should be addressed to N. Ashgriz at ashgriz@mie.utoronto.ca.

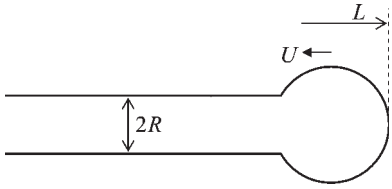

Figure 1. Schematic showing part of a liquid ligament with total length *L*.

obtained. However, results on the contraction of free ligaments (e.g., length as a function of time) in the past numerical and experimental works are limited.

Schulkes[18] presented numerical results of the length of symmetric ligaments as a function of time (Figure 8 in Schulkes[18]). The ligaments with $Oh = 1$ were shown to contract with almost constant accelerations for $t > \sim 0.01 t_c$, where t_c is capillary time scale expressed by

$$t_c = \sqrt{\frac{\rho R^3}{\sigma}}. \tag{1}$$

Carrying out simple derivation to the results in Schulkes,[18] we can get

$$-\frac{d^2 L(t)}{dt^2} \sim \frac{2L_0}{t_c^2}, \tag{2}$$

where L is the length of the ligament (see Figure 1) as a function of time t, and L_0 is the initial length. On the basis of self-similar solutions to Navier-Stokes equations for pinch-off problems, Eggers[20] proposed that the retraction of one free end of the liquid ligament after pinch-off can be approximated by

$$U(t) \sim 8.7\sqrt{\frac{\mu}{t\rho}}. \tag{3}$$

However, this equation can only be used for time and distance close to the pinch-off point, i.e., $t < t_v$, $\Delta L < L_v$. Here, ΔL is the distance from the pinch-off point, while t_v and L_v are the viscous time scale and length scale, respectively, given by

$$t_v = \frac{\mu^3}{\rho\sigma^2} \tag{4}$$

and

$$L_v = \frac{\mu^2}{\rho\sigma}. \tag{5}$$

Kowalewski[21] experimentally studied the ligament retraction as a result of the separation of droplets from pulsed jets of varied fluids, and used Eq. 3 to compare with observed velocity ranges. It was found that Eq. 3 did not match the experimental results. In contrast, the observed velocities showed that

$$U \sim O(U_c), \tag{6}$$

where U_c is a characteristic velocity defined as

$$U_c = \sqrt{\frac{\sigma}{\rho R}} = \frac{R}{t_c}. \tag{7}$$

Dupré[16] studied the rupture of inviscid films using energy balance, and obtained an expression for the rim velocity. If the film thickness in the expression is replaced with the ligament radius R, based on his method, the retraction velocity of ligament end is

$$U = 2U_c. \tag{8}$$

Keller[22] proposed a simplified model, in which the ligament end is assumed to be a blob connected to an inviscid column, as shown in Figure 1. In the case that the liquid column is of uniform radius, the model predicts that the blob recedes at a uniform velocity given by

$$U = \sqrt{2}U_c. \tag{9}$$

Equation 9 agrees with the theories of Taylor[14] and Culick[15] on the motion of free rim of liquid sheets and films, which balance the surface tension force ($2\pi R\sigma$) and momentum force ($-\rho U^2 \pi R^2$). However, this force balance is questionable, because the capillary pressure force ($-\pi R\sigma$) was not included. Carrying out force balance to the three forces above, we obtain

$$U = U_c. \tag{10}$$

This force balance resembles a general analysis of force balance on stretching jets in Roisman.[13]

Equations 8–10 provides different expressions for the retraction velocity of one free end of the ligament, which are independent of blob size and time. These expressions may be useful for a rough estimate of time scale for ligament contraction. However, they cannot be used to accurately predict the time taken for the ligament to complete contraction process, especially for ligaments with two free ends and different initial blob sizes. One major reason is that the contraction is not necessarily with constant velocity due to the growth of the blobs at the ends of the ligament. Our study will show that the predictions of ligament lifetime based on Eqs. 8–10 differ significantly from our experimental and theoretical results. In this work, we experimentally measure the transient length of a liquid ligament produced using an ink-jet printer. An analytical model based on the conservation of mass, momentum, and energy is developed to predict the ligament length as a function of time, thereby predicting the lifetime of the ligament. The results of the model are compared with our experimental results.

Experimental Setup

A commercial solid-inkjet printhead with "bend mode"[23] (Figure 2a) piezo-electrically driven droplet-on-demand (DOD), with orifice radius 10 μm, was used to eject ink droplets. The printhead is highly repeatable in its jetting process, which has been proven in our preliminary tests. Figure 2a shows the schematic of a solid-inkjet printer[24] in which the piezoelectric printhead deposits molten ink drop-

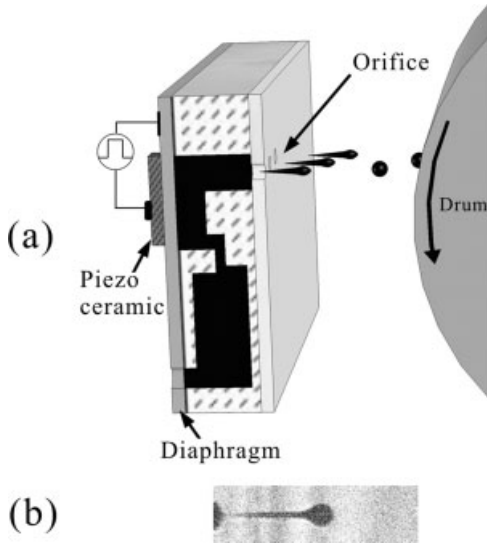

Figure 2. (a) In a solid-inkjet printer, ink droplets are generated from a piezo-electrically driven DOD printhead and are deposited on a rotating drum to print images; (b) when an electric pulse is applied, a liquid ligament is generated.

lets on an intermediate drum. When an electric pulse is applied, ink is ejected out of small orifices (10 μm in radius) due to the pressure generated by a voltage-pulse driven piezoelectric actuator. The ejected ink separates from the remaining liquid in the orifice, generating a liquid ligament in flight (Figure 2b). Without external restraint forces, the liquid ligament will relax to form a spherical body so that the surface energy can be minimized. ColorStix 8200 (Xerox Corporation, Rochester, NY), a commonly used commercial wax-based ink, was used. The ink was melted in the printhead and ejected with an initial temperature of 140°C. The properties of the ink at 140°C are as follows: density $\rho = 820$ kg/m^3, viscosity $\mu = 0.0105$ Pa s, and surface tension $\sigma = 0.02869$ N/m. Our estimate shows that the droplet temperature decreases to ~130°C after traveling 2 mm. Because this temperature is still well above the melting temperature of the ink (~95°C) and ink properties do not change appreciably in this temperature range, the effect of temperature change will not be considered in this article.

The printhead was placed such that the ink was ejected horizontally. Because the Froude number is in the order of 10^4, gravitational effect is negligible. The jetting process was constructed based on a sequence of photographs taken with strobe-photography method, which is able to resolve fast dynamic processes. Each picture was taken with a different delay in time between the triggers to the printhead and camera. A digital camera (D100, Nikon) was used together with microscope lens (QM100, Questar) to take photographs. The strobe lighting source used is a gas discharge lamp (Nanolite, High-Speed Photo-Systeme, Wedel, Germany), which can provide flashes with duration of 11 ns. The time accuracy in the strobe-photography method was around 1 ns.

Experimental Observation

Time evolution of droplet formation upon application of a pulsed force on the liquid chamber is shown in Figure 3. The jetting process started with the appearance of outward moving meniscus ($t = 0$ μs), which kept growing into a ligament connected to the orifice. The ligament separated from the remaining liquid in the orifice, contracted and eventually formed a droplet.

It is evident that, for one single pulse, droplets were formed as a result of ligament contraction. The ligament detached from the remaining liquid in the orifice with a conical tip, due to the abrupt stop of liquid motion inside the nozzle. This conical point quickly formed a round end, due to local sharp curvature. The ligament formed contracted into droplets without breakup. Although the ligament length is much larger than the cutoff wavelength of capillary instability $2\pi R$, no capillary waves or end-pinching were observed on the surface of the ligament. In this work, $Oh \sim 1$ for $R \sim 5$ μm, approximately in the range of stable contraction proposed by Schulkes.[18] Additionally, the fluid viscosity was 10^2 times larger than that of surrounding air, which indicates negligible resistance from the ambient air.[10]

The contraction of ligaments has been found to play a major role in the process of droplet formation. The photographs shown in Figure 3 were processed and measured using image analysis software, ImageJ (National Institute of Mental Health, Bethesda, MD). Figure 4 shows the locations

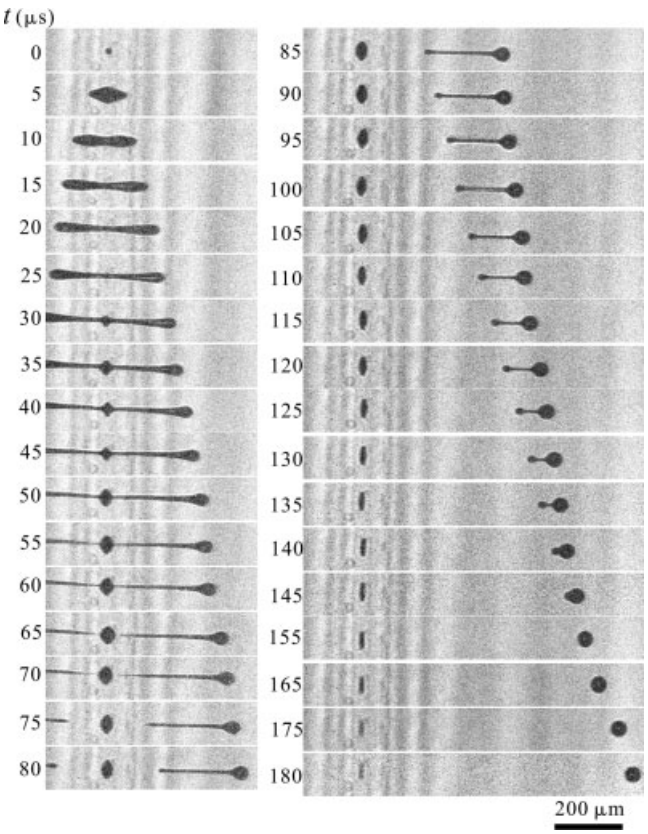

Figure 3. Time sequence of droplet formation in response to one electric pulse with pulse duration of 8 μs and voltage amplitude of 29 volts.

The ink is ejected rightward.

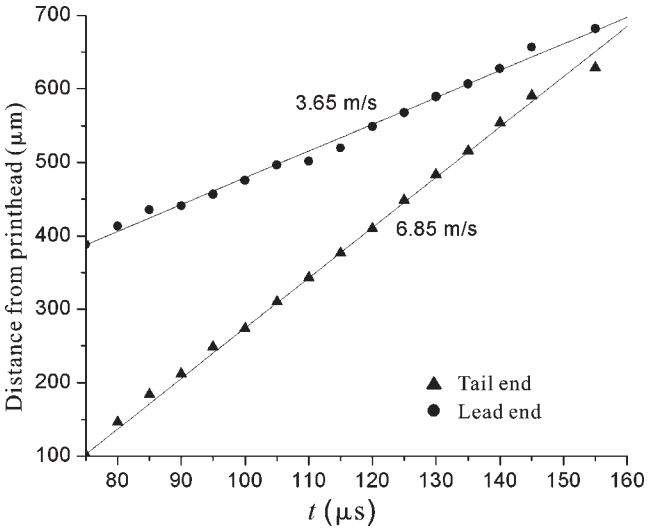

Figure 4. Locations of lead and tail ends of the ligament relative to the printhead after detaching from the orifice.

Velocities shown are the linear slopes of the data points.

of the lead and tail ends of the ligament relative to the printhead as a function of time. Carrying out linear fittings, the relative velocity between the two ends is ~3.2 m/s.

Theoretical Consideration of Ligament Contraction

Because the liquid ligament observed in this work flew in the air, the effect of air drag needs to be evaluated first. Air drag on a rigid spherical body is considered. The Reynolds number based on the properties of ambient air ($\rho_g = 1$ kg/m^3, $\mu_g = 20.94 \times 10^{-6}$ Pa s for air at 80°C, an average of the printhead and room temperatures), velocity ($U_j \sim 5$ m/s), and diameter ($D \sim 40$ μm) of the lead end of the ligament is

$$Re = \frac{DU_j\rho_g}{\mu_g}.$$

Because $Re < 10$ in our tests, the following correlation for drag coefficient[25] can be used,

$$C_d = \frac{24}{Re}\left[1 + 0.1315Re^{(0.82-0.05\log_{10}^{Re})}\right]. \quad (11)$$

The deceleration rate due to air drag is expressed by

$$a_d = 0.75C_d\frac{\rho_g}{D\rho}U_j^2. \quad (12)$$

Our estimate shows $a_d \sim 10^3$ m/s^2. For a time period of 100 μs, longer than the contraction time shown in Figure 3, the air drag can cause the velocity to change by 0.1 m/s, much smaller than the relative velocity shown in Figure 4. Therefore, the ligament in question can be considered as a free ligament subject to no external forces.

To develop an analytical model to estimate the contraction time scale of free ligaments, we make four important simplifying assumptions: (1) at $t = 0$, there are two blobs at the ends of the ligament; (2) the radius of the central column remains constant and uniform during the contraction process; (3) energy dissipation due to viscous effect is negligible; (4) the ligament remains stable during contraction. The second assumption agrees with the observation shown in Figure 3. This implies that the flow field inside the column is weak, showing very small velocities as compared with those of the two blobs.[9] The flow driven by the pressure difference between the blobs and the central column might be appreciable at the blob-column interface. However, the local fluid velocity is counteracted by the retraction of the blobs, thereby maintaining constant radius of the central column. The weak flow inside the column makes the third assumption hold.

Choosing the earth as the frame of reference, the ligament with two spherical blobs of arbitrary sizes can be divided into three control volumes as shown in Figure 5: control volume #1 (CV1) with radius R_1 and velocity U_1; CV2 with R_2 and U_2; and the central column CV3 with R and U_3. Different from Figure 1 where L is the total length of the ligament, here L is used to represent the length of the central column, excluding the blobs at the ends of the ligament.

Applying conservation of mass gives

$$\frac{d}{dt}\sum_{i=1,2,3} V_i = 0, \quad (13)$$

where the volumes of the three control volumes are

$$\begin{aligned} V_1 &= V_{1,0} + \pi R^2\int_0^t (U_1 + U_3)dt, \\ V_2 &= V_{2,0} + \pi R^2\int_0^t (U_2 - U_3)dt, \\ V_3 &= \pi R^2 L. \end{aligned} \quad (14)$$

The velocities U_1, U_2, and U_3 are used as scalars. The initial volumes of the two blobs, $V_{1,0}$ and $V_{2,0}$, are given by

$$V_{i,0} = \frac{4}{3}\pi R_{i,0}^3. \quad (15)$$

Substituting Eq. 14 into Eq. 13, we get

$$L = L_0 - \int_0^t (U_1 + U_2)dt, \quad (16)$$

where L_0 is the length of the central column at $t = 0$. And the radii of the two blobs are given by

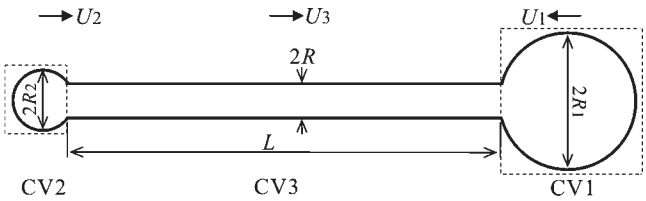

Figure 5. A liquid ligament can be modeled as a liquid column with two blobs at its ends.

$$R_{i=1,2} = \left(\frac{3}{4\pi}V_i\right)^{1/3}. \tag{17}$$

The free ligament is a closed system, which has no interactions with the surroundings. Therefore, to satisfy the conservation of momentum and the conservation of energy, we require

$$\frac{d}{dt}\sum_{i=1,2,3} V_i\vec{U}_i = 0 \tag{18}$$

and

$$\sum_{i=1,2,3}\frac{d}{dt}(\mathrm{SE}_i + \mathrm{KE}_i) = 0, \tag{19}$$

where SE and KE represent surface energy and kinetic energy, respectively.

However, there are four unknowns L, U_1, U_2, and U_3 in three equations. Because we are concerned only with U_1 and U_2, a further simplification can be made choosing the central column as the frame of reference by setting $U_3 = 0$, i.e., the center of mass of the central column remains constant in space and time. Because the free ligament has zero momentum in the reference frame attached to its center of mass, Eq. 18 can be changed to

$$\frac{U_1}{U_2} = \frac{V_{2,0} + \pi R^2\int_0^t U_2 dt}{V_{1,0} + \pi R^2\int_0^t U_1 dt}. \tag{20}$$

The surface energy terms in Eq. 19 are

$$\begin{aligned}&\mathrm{SE}_{i=1,2} \sim \sigma\left(4\pi R_i^2 - \pi R^2\right)\\ &\mathrm{SE}_3 = 2\pi RL\sigma\end{aligned}. \tag{21}$$

The kinetic energy terms in Eq. 19 are

$$\begin{aligned}&\mathrm{KE}_3 = 0\\ &\mathrm{KE}_{i=1,2} = \frac{1}{2}\rho V_i U_i^2 + \mathrm{IE}_i.\end{aligned} \tag{22}$$

where IE_i is internal kinetic energy due to the growth of the two blobs. To find this term, the blob growth can be modeled as a growing droplet suspended from a circular tube with radius R and fluid velocity U_i, as sketched in Figure 6a. This can also be further modeled as a spherical source with diameter R and fluid velocity U_i and concentric with the blob, as shown in Figure 6b. Continuity requires

$$U_i\pi R^2 = u4\pi r^2 = \frac{dR_i}{dt}4\pi R_i^2, \tag{23}$$

where u is the radial velocity at radius r in the blob. Therefore, the internal kinetic energy is expressed by

$$\mathrm{IE}_i = \int_{R/2}^{R_i}\frac{\rho}{2}4\pi r^2 u^2 dr = \rho\frac{\pi R^4}{8}\left(\frac{2}{R} - \frac{1}{R_i}\right)U_i^2. \tag{24}$$

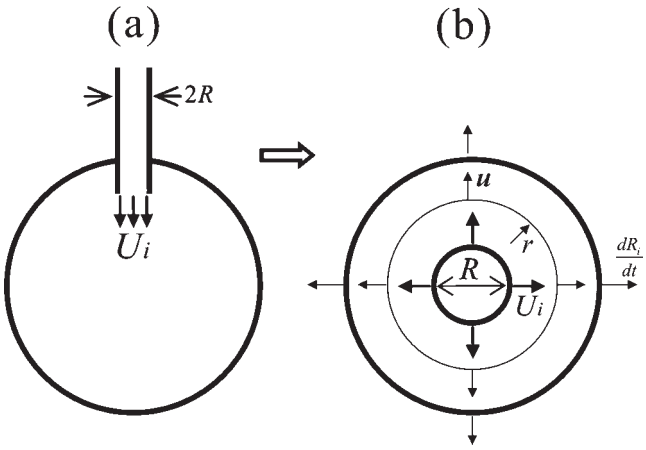

Figure 6. (a) The growth of blobs can be modeled as a growing drop suspended from a circular tube; (b) the growing pendant drop can be modeled as a drop with a concentric, spherical source.

Substituting Eqs. 21, 22, and 24 into Eq. 19 gives

$$\sum_{i=1,2} U_i\left\{\left(\frac{4}{3}R_i^3 + \frac{R^3}{2} - \frac{R^4}{4R_i}\right)\frac{dU_i}{dt} + \frac{R^2}{2}\left(1 + \frac{R^4}{16R_i^4}\right)U_i^2 + \frac{2R\sigma}{\rho}\left(\frac{R}{R_i} - 1\right)\right\} = 0, \tag{25}$$

where, from Eq. 17,

$$R_i = \left(\frac{3}{4}\right)^{1/3}\left(\frac{V_{i,0}}{\pi} + R^2\int_0^t U_i dt\right)^{1/3}. \tag{26}$$

Combining Eqs. 20 and 25, we can solve for transient velocities U_1 and U_2, which can be put into Eq. 16 to calculate the transient length of the central column.

To obtain a nondimensional solution to this problem, we normalize the lengths and radii with R, velocities with U_c, and time with t_c, i.e., $\overline{L} = L/R$; $\overline{L}_0 = L_0/R$; $\overline{R}_{i,0} = R_{i,0}/R$; $\overline{U}_i = U_i/U_c$; $\bar{t} = t/t_c$. Applying these normalized parameters to Eqs. 16, 20, and 25, 26, we obtain

$$\overline{L}/\overline{L}_0 = 1 - \frac{1}{\overline{L}_0}\int_0^{\bar{t}}\left(\overline{U}_1 + \overline{U}_2\right)d\bar{t}$$

$$\frac{\overline{U}_1}{\overline{U}_2} = \frac{\frac{4}{3}\overline{R}_{2,0}^3 + \int_0^{\bar{t}}\overline{U}_2 d\bar{t}}{\frac{4}{3}\overline{R}_{1,0}^3 + \int_0^{\bar{t}}\overline{U}_1 d\bar{t}}$$

$$\sum_{i=1,2}\overline{U}_i\left\{\left(\frac{4}{3}\overline{R}_i^3 + \frac{1}{2} - \frac{1}{4\overline{R}_i}\right)\frac{d\overline{U}_i}{d\bar{t}} + \frac{1}{2}\left(1 + \frac{1}{16\overline{R}_i^4}\right)\overline{U}_i^2 + 2\left(\frac{1}{\overline{R}_i} - 1\right)\right\} = 0$$

$$\overline{R}_i = \left(\overline{R}_{i,0}^3 + \frac{3}{4}\int_0^{\bar{t}}\overline{U}_i d\bar{t}\right)^{1/3}. \tag{27}$$

Discussion

In our tests, the radius of the central column R was measured to be 5 μm. To satisfy the assumed initial shape of the ligament, the ligament at 75 μs in Figure 3 ($L_0 = 220$ μm, $R_{1,0} = 20$ μm, $R_{2,0} = 5$ μm) is chosen to be the initial point. Hence the initial conditions are $\overline{L}_0 = 44$, $\overline{R}_{1,0} = 4$, and $\overline{R}_{2,0} = 1$. Our experimental observation shows that the ligament detached from the orifice with a conical tip, which restored into a small blob. Because of this restoration process, the initial velocities of the two blobs $U_{1,0}$ and $U_{2,0}$ were not zero at 75 μs in Figure 3. We assume the tail blob of radius R is formed from a cone with base radius R and half volume of the blob. Without considering viscous dissipation, the conservation of energy gives

$$\sigma\left(\sqrt{5}-2\right)\pi R^2 = \frac{1}{2}\rho V_{2,0}U_{2,0}^2. \tag{28}$$

The left-hand side is the change of surface energy, whereas the right-hand side is the kinetic energy of the blob. Solving Eq. 28 for $U_{2,0}$ in the nondimensional form gives

$$\overline{U}_{2,0} = \sqrt{\frac{3}{2\overline{R}_{2,0}^3}\left(\sqrt{5}-2\right)}. \tag{29}$$

Applying conservation of momentum, the initial velocity of CV1 is

$$\overline{U}_{1,0} = \left(\frac{\overline{R}_{2,0}}{\overline{R}_{1,0}}\right)^3 \overline{U}_{2,0}. \tag{30}$$

Figure 7 shows the theoretical model in comparison with experimental results measured from Figure 3. The ratio of transient length to initial length $\overline{L}_0/\overline{L}_0$ is plotted as a function of dimensionless time $\bar{t}$. The time taken for the ligament to contract is theoretically predicted to be ~31 and is experimentally measured to be ~34, showing good agreement.

Recall that the theoretical model developed above did not consider viscous dissipation. However, at the later stage of the contraction the two blobs approached closer, the viscous effect might increase considerably due to the increase of velocity gradient in the central column in the direction of contraction. The experimental data presented in Figure 7 show a smaller slope (lower velocity) at the end of contraction process than that at the early portion of the process. This explanation also can find support from the numerical results of velocity distribution in Stone and Leal[9] for a symmetric ligament contracting in an ambient, quiescent fluid with much lower viscosity.

Figure 7 also compares our experimental and theoretical results with the results of constant velocity theories Eqs. 8–10. If the two blobs retract with equal velocity, which is independent of time and blob size, the length as a function of time can be expressed as

$$\overline{L}/\overline{L}_0 = 1 - \frac{2\overline{U}}{\overline{L}_0}\bar{t}. \tag{31}$$

Figure 7 shows that using the constant velocities given by Eqs. 8–10 predicts much faster contraction processes and results in significant errors.

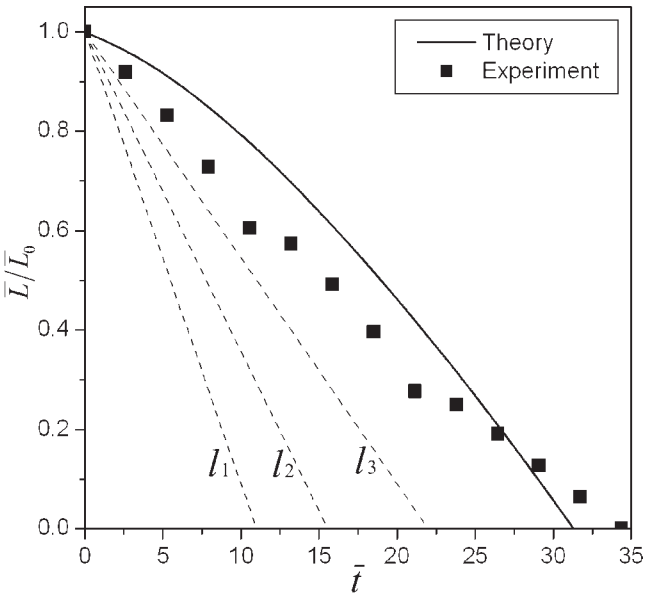

Figure 7. Theoretical Eq. 27 and experimental results of ligament length as function of time.

The dashed lines are based on Eq. 31 using constant velocities given by Eqs. 8–10: l_1 for Eq. 8; l_2 for Eq. 9; l_3 for Eq. 10.

The initial length of the ligament in our test was longer than the cutoff wavelength of the Rayleigh instability,[26] since $\overline{L}_0 > 2\pi$. However, the ligament remained stable while contracting into a droplet. The characteristic time of breakup of infinite inviscid liquid jets for the fastest growing wavelength is given by[27]

$$\bar{t}_{\text{inv}} = \frac{1}{0.3433}, \tag{32}$$

where $\bar{t}_{\text{inv}}$ is a dimensionless time normalized by t_c. For highly viscous jets this characteristic time is approximately expressed by[27]

$$\bar{t}_{\text{visc}} = 6\text{Oh}, \tag{33}$$

where $\bar{t}_{\text{visc}}$ is a dimensionless time normalized by t_c. For the ligament in consideration, $\bar{t}_{\text{visc}} \sim 6$.

Comparing Eqs. 32 and 33 with the results shown in Figure 7, the contraction time is longer than the breakup time scales for inviscid and viscous jets. Nonetheless, no capillary waves were observed on the surface of the ligament during contraction (Figure 3). The capillary instability time scale depends on the introduced perturbation in the numerical study and determination of initial perturbation in experiments. Decrease of the initial amplitude leads to substantial increase of time scale. It should also be noted that the basic flow of Rayleigh instability features a uniform velocity distribution across any section along the infinite jet, and the theory is independent of inertial forces.[28] The flow inside a free ligament with finite length during contraction differs significantly from that of Rayleigh jets. Therefore, additional work is needed in future to address the effect of flow in causing the instability of liquid ligaments.

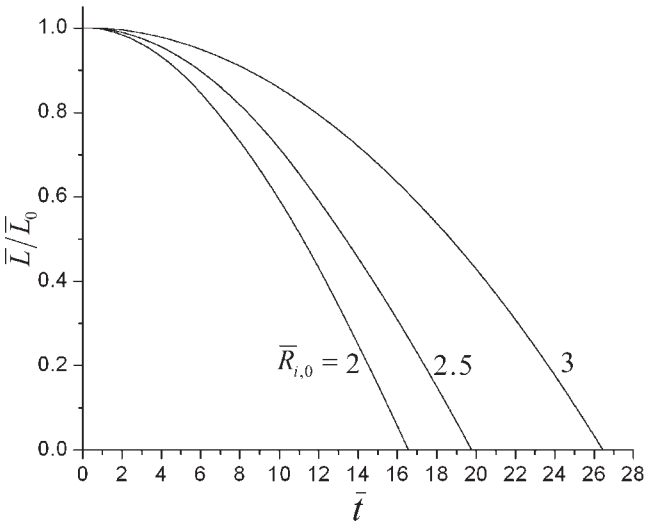

Figure 8. Contraction of liquid ligaments with varied initial radii of the blobs but the same initial length $\overline{L}_0 = 20$.

The initial radii of the two blobs are equal.

The theoretical model proposed in this work is dependent on the blob size. The variation of contraction time with the dimensions of the ligament can be evaluated by considering symmetric ligaments, where the two blobs have identical size. The initial velocities of the two blobs are assumed to be zero. Figure 8 shows the contraction of ligaments with varied blob radii but the same initial length $\overline{L}_0 = 20$. The contraction time increases with the initial blob size, increasing from ~17 for $\overline{R}_{i,0} = 2$ to ~26 for $\overline{R}_{i,0} = 3$.

Conclusions

The contraction of liquid ligaments was studied, and a theoretical model was developed to predict the time for contraction. The ligament was considered inviscid and free of external forces. Additionally, the ligament was assumed to be stable during contraction. The model was based on the conservation of mass, momentum and energy. Theoretical analysis showed that the contraction time increases with the initial radius of the blobs. The model was compared with our experiments on the droplet formation from a piezo-electric inkjet printhead. A liquid ligament was formed when the printhead was driven by an electric pulse, and the contraction of the ligament was measured. The experimental results showed good agreement with the theoretical predictions. Our theoretical and experimental results were also compared with those of constant contraction velocity theories. It was found that all the contraction velocities proposed in literature predict much faster contraction, resulting in significant errors.

Acknowledgments

The authors are indebted to Dr. Stephan Drappel and Chris Wagner from Xerox Research Centre of Canada and Bradley Gerner from Xerox Corporation for their assistance in setting up the jetting fixture. This work is supported by Xerox Foundation and Natural Sciences and Engineering Research Council of Canada (NSERC).

Notation

a_d = deceleration rate
C_d = drag coefficient
D = diameter of lead end of ligament
IE_i = internal kinetic energies of blobs ($i = 1, 2$)
KE_i = kinetic energies of blobs ($i = 1, 2$) and central column ($i = 3$)
L = length of ligament
L_v = viscous length scale
ΔL = distance from pinch-off point
r = radial coordinate
R = radius of central column of ligament
R_i = radii of blobs ($i = 1, 2$)
SE_i = surface energies of blobs ($i = 1, 2$) and central column ($i = 3$)
t = time
t_c = capillary time scale
t_{inv} = characteristic breakup time of inviscid jets
t_v = viscous time scale
t_{visc} = characteristic breakup time of highly viscous jets
u = fluid velocity inside blobs
U = retraction velocity of ligament ends
U_c = characteristic velocity associated with surface tension
U_i = velocities of blobs ($i = 1, 2$) and central column ($i = 3$)
U_j = velocity of ligament traveling in air
V_i = volumes of blobs ($i = 1, 2$) and central column ($i = 3$)

Nondimensional numbers

Oh = Ohnesorge number
Re = Reynolds number

Greek letters

μ = viscosity
σ = surface tension
ρ = density

Embellishment

upper bar = nondimensional

Subscripts

0 = initial
g = ambient air

Literature Cited

1. Bogy DB, Talke PE. Experimental and theoretical study of wave propagation phenomena in drop-on-demand ink jet devices. *IBM J Res Dev*. 1984;28:314–321.
2. Cheng S, Chandra S. A pneumatic droplet-on-demand generator. *Exp Fluids*. 2003;34:755–762.
3. Ambravaneswaran B, Phillips SD, Basaran O. A. Theoretical analysis of a dripping faucet. *Phys Rev Lett*. 2000;85:5332–5335.
4. Shi XD, Brenner MP, Nagel SR. A cascade of structure in a drop falling from a faucet. *Science*. 1994;265:219–222.
5. Zhang X, Basaran OA. An experimental study of dynamics of drop formation. *Phys Fluids*. 1995;7:1184–1203.
6. Henderson DM, Pritchard WG, Smolka LB. On the pinch-off of a pendant drop of viscous fluid. *Phys Fluids*. 1997;9:3188–3200.
7. Taylor GI. The formation of emulsions in definable fields of flow. *Proc R Soc London Ser A*. 1934;146:501–523.
8. Stone HA, Bentley BJ, Leal LG. An experimental study of transient effects in the breakup of viscous drops. *J Fluid Mech*. 1986;173:131–158.
9. Stone HA, Leal LG. Relaxation and breakup of an initially extended drop in an otherwise quiescent fluid. *J Fluid Mech*. 1989;198:399–427.
10. Stone HA. Dynamics of drop deformation and breakup in viscous fluids. *Annu Rev Fluid Mech*. 1994;26:65–102.
11. Ashgriz N, Poo JY. Coalescence and separation in binary collision of liquid drops. *J Fluid Mech*. 1990;221:183–204.

12. Qian J, Law CK. Regimes of coalescence and separation in droplet collision. *J Fluid Mech*. 1997;331:59–80.
13. Roisman IV. Dynamics of inertia dominated binary drop collisions. *Phys Fluids*. 2004;16:3438–3449.
14. Taylor GI. The dynamics of thin sheets of fluid. III. Disintegration of fluid sheets. *Proc R Soc London Ser A*. 1959;253:313–321.
15. Culick FEC. Comments on a ruptured soap film. *J Appl Phys*. 1960;31:1128–1129.
16. Dupré A. Theorie mécanique de la chaleur. *Ann Chim Phys*. 1867;4:194–220.
17. Eggers J, Dupont TF. Drop formation in a one-dimensional approximation of the Navier-Stokes equation. *J Fluid Mech*. 1994;262:205–221.
18. Schulkes RMSM. The contraction of liquid filaments. *J Fluid Mech*. 1996;309:277–300.
19. Brenner MP, Eggers J, Joseph K, Nagel SR, Shi XD. Breakdown of scaling in droplet fission at high Reynolds number. *Phys Fluids*. 1997;9:1573–1590.
20. Eggers J. Theory of drop formation. *Phys Fluids*. 1995;7:941–953.
21. Kowalewski TA. On the separation of droplets from a liquid jet. *Fluid Dyn Res*. 1996;17:121–145.
22. Keller JB. Breaking of liquid films and threads. *Phys Fluids*. 1983;26:3451–3453.
23. Le HP. Progress and trends in ink-jet printing technology. *J Imaging Sci Technol*. 1998;42:49–62.
24. Snyder T, Korol S. Modeling the offset solid-ink printing process. *Int Conf Digit Print Technol*. 1997;13:709–715.
25. Clift R, Grace JR, Weber ME. *Bubbles, Drops, and Particles*. New York: Academic Press, 1978:112.
26. Rayleigh L. On the instability of jets. *Proc R Soc London Ser A*. 1878;10:4–13.
27. Chandrasekhar S. *Hydrodynamics and Hydromagnetic Stability*. New York: Dover Publications Inc., 1981:538–542.
28. Lin SP. *Breakup of Liquid Sheets and Jets*. Cambridge: Cambridge University Press, 2003.

Manuscript received Dec. 18, 2007, revision received Apr. 16, 2008, and final revision received July 17, 2008.